Acta Crystallographica Section D
Biological Crystallography
ISSN 0907-4449

$NADP^+$ and NAD^+ binding to the dual coenzyme specific enzyme *Leuconostoc mesenteroides* glucose 6-phosphate dehydrogenase: different interdomain hinge angles are seen in different binary and ternary complexes

Claire E. Naylor,[a]† Sheila Gover,[a] Ajit K. Basak,[a]† Michael S. Cosgrove,[b]‡ H. Richard Levy[b] and Margaret J. Adams[a]*

[a]Laboratory of Molecular Biophysics, Department of Biochemistry, University of Oxford, Rex Richards Building, South Parks Road, Oxford OX1 3QU, England, and [b]Department of Biology, Syracuse University, Syracuse, New York 13244, USA

† Current address: Department of Crystallography, Birkbeck College, Malet Street, London WC1E 7HX, England.
‡ Current address: Department of Biophysics and Biophysical Chemistry, Johns Hopkins School of Medicine, 725 North Wolfe Street, Baltimore, Maryland 21205, USA.

Correspondence e-mail: margaret@biop.ox.ac.uk

Received 21 November 2000
Accepted 19 February 2001

PDB References: NADP, 1h9a; $P6_222$-empty, 1h9b; NAD, 1h94; C2-empty, 1h93.

The reduced coenzymes NADH and NADPH only differ by one phosphate, but in the cell NADH provides reducing power for catabolism while NADPH is utilized in biosynthetic pathways. Enzymes almost invariably discriminate between the coenzymes, but glucose 6-phosphate dehydrogenase (G6PD) from *Leuconostoc mesenteroides* is rare in being functionally dual specific. In order to elucidate the coenzyme selectivity, the structures of $NADP^+$- and NAD^+-complexed *L. mesenteroides* G6PD have been determined including data to 2.2 and 2.5 Å resolution, respectively, and compared with unliganded G6PD crystallized in the same space groups. Coenzyme binding is also compared with that in a ternary complex of a mutant in which Asp177 in the active site has been mutated to asparagine. There are no gross structural differences between the complexes. In both binary complexes, the enzyme interdomain hinge angle has opened. $NADP^+$ binds to the furthest open form; of the residues within the coenzyme domain, only Arg46 moves, interacting with the 2′-phosphate and adenine. NAD^+ is less well defined in the binding site; smaller hinge opening is seen but larger local changes: Arg46 is displaced, Thr14 bonds the 3′-hydroxyl and Gln47 bonds the 2′-hydroxyl. In the ternary complex, the hinge angle has closed; only the adenine nucleotide is ordered in the binding site. Arg46 again provides most binding interactions.

1. Introduction

Glucose 6-phosphate dehydrogenase (G6PD; E.C. 1.1.1.49) is the first enzyme of the pentose phosphate pathway and in many organisms, including mammals, is $NADP^+$ dependent. For these species, G6PD, together with 6-phosphogluconate dehydrogenase (6PGDH), the second dehydrogenase of the pathway, generates NADPH for reductive biosynthesis or to combat oxidative stress (Levy, 1979; Rosemeyer, 1987).

G6PD from the microorganism *L. mesenteroides* has dual coenzyme specificity. In both the $NADP^+$ and the NAD^+ reaction, hydrogen is added to the *Si* face; transferred nuclear Overhauser enhancement has demonstrated that the nicotinamide has the *syn* conformation, but has also shown some differences between the bound conformations of the two coenzymes (Levy, Ejchart *et al.*, 1983). The reduced coenzymes take part in different metabolic pathways in *L. mesenteroides*: NADPH is used in reductive biosynthesis of fatty acids (Kemp & Rose, 1964), while NADH is used in

heterolactic fermentation to provide ethanol, lactic acid and carbon dioxide (De Moss *et al.*, 1951). Such dual specificity is unusual, not only for G6PD, but for nicotinamide nucleotide dehydrogenases generally. Attempts to change the coenzyme specificity of dehydrogenases by site-directed mutagenesis have so far only succeeded when a large number of residues in the binding site have been changed (Hurley *et al.*, 1996; Scrutton *et al.*, 1990).

In an effort to understand the basis of dual-nucleotide specificity, the kinetic mechanism of *L. mesenteroides* G6PD has been studied in detail (reviewed in Levy, 1989). There is no evidence of cooperativity for this dimeric enzyme; K_m for $NADP^+$ (8 μM) is 20-fold lower than for NAD^+ and k_{cat}/K_m is 10-fold higher. While K_d for $NADP^+$ is similar to K_m, it is higher for NAD^+ (3000 μM), 300 times that for $NADP^+$. The kinetic mechanism differs in the $NADP^+$- and NAD^+-dependent reactions; the $NADP^+$ reaction is ordered-sequential with coenzyme binding first, while the NAD^+ reaction shows steady-state random kinetics (Levy, Christoff *et al.*, 1983). High concentrations of glucose 6-phosphate (G6P) or a high NADPH:$NADP^+$ ratio are expected and have been shown to favour the NAD^+-dependent reaction (Levy & Daouk, 1979; Levy *et al.*, 1979). Protein fluorescence is quenched when either coenzyme binds; the greater magnitude of fluorescence quenching has been interpreted as evidence that a larger protein conformation change occurs when NAD^+ binds (Haghighi & Levy, 1982; Levy, 1989).

The *L. mesenteroides* enzyme has been cloned and expressed in *E. coli* (Lee *et al.*, 1991). It was crystallized from phosphate in the absence of coenzyme or substrate and its structure, referred to hereafter as 'G6PD-P', was solved at 2.0 Å resolution (Rowland *et al.*, 1994). The wild-type enzyme lacks cysteine residues. In an effort to generate heavy-atom sites for isomorphous replacement, a variety of site-directed mutants which introduced single cysteines were made; these include the mutants Q365C and S215C, both of which are active. They crystallize under the same conditions as the wild-type enzyme but diffract to higher resolution (Adams *et al.*, 1993), making them preferred for the crystallographic studies described in this paper.

The structure of the G6PD-P dimer shows its two subunits to be related by a non-crystallographic twofold axis which is not exact. The monomer has two domains: a coenzyme-binding domain with a Rossmann fold and a larger $\beta + \alpha$ domain which forms the dimer interface and contains a large antiparallel sheet in the form of a half barrel. A highly conserved eight-residue peptide (175–182), which includes a lysine (182) shown to be essential in the human enzyme (Camardella *et al.*, 1988), is at the domain boundary. Two phosphate ions bind to His178 of this peptide in the *A* subunit of G6PD-P, while in the *B* subunit one phosphate is bound. These subunits are hereafter called the AP and BP subunits. Asp177 makes a hydrogen bond to a conserved histidine (240) which has been shown by site-directed mutagenesis to be the essential base for the enzyme reaction (Cosgrove *et al.*, 1998). In subunit BP, a conserved proline (149) is seen to have a *trans* conformation, while in subunit AP it is *cis*. This difference affects the orientation of the residues of the following helix (αe) and makes a small change to the angle between the two domains. Binding of the substrate G6P has been described both in a binary complex of the mutant Q365C and in a ternary NADPH–G6P complex of the active-site mutant D177N (Cosgrove *et al.*, 2000).

The probable coenzyme-binding site was predicted from the G6PD-P structure. The 177-residue coenzyme-binding domain of G6PD is larger than the typical 130–140 residue NAD^+- or $NADP^+$-binding domain. There are no additional secondary-structural elements in the domain, but most helices have an additional turn.

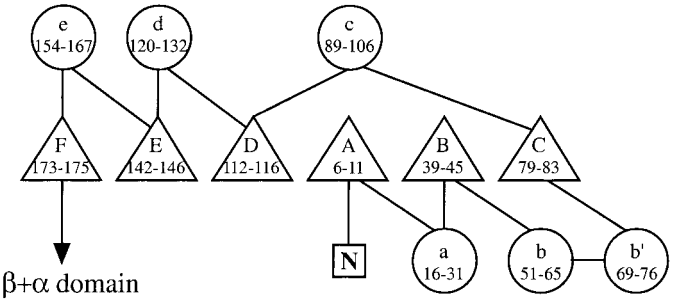

The standard dinucleotide-binding fingerprint (G*X*G*XX*G/A) is modified to GgtGDLa (residues 12–18; those in upper case are conserved for all known species) and is positioned at the βA–αa tight turn and the first turn of αa. Helix αa is bent by a conserved proline. A conserved arginine (46) on the turn following the sheet strand βB has been shown by site-directed mutagenesis to be more important in binding $NADP^+$ than in binding NAD^+ (Levy *et al.*, 1996). Our experiments to diffuse either $NADP^+$ or NAD^+ into crystals grown from phosphate were unsuccessful.

This paper describes the cocrystallization of *L. mesenteroides* G6PD with $NADP^+$ and with NAD^+; two different precipitants were used, neither of which was phosphate. Crystals of the enzyme which do not have coenzyme bound were also grown under each condition and appeared to be isomorphous with the corresponding coenzyme-bound crystals. The binding of reduced coenzyme in the ternary complex of the active-site mutant D177N with G6P and NADPH (Cosgrove *et al.*, 2000) is compared in this paper with $NADP^+$ and NAD^+ binding in binary complexes of the active enzyme. Comparisons of the coenzyme-binding sites and of the enzyme conformations for the different complexes and crystal forms are made and their contribution to understanding discrimination between the coenzymes and dual specificity in this enzyme is discussed.

2. Materials and methods

2.1. Expression and purification

All protein was expressed and purified in the Syracuse laboratory according to the methods described previously (Lee & Levy, 1992). All chemicals were purchased from Sigma unless otherwise stated.

Table 1
X-ray data-collection statistics.

Values in parentheses refer to the highest resolution shell.

Data set	*A*1, NADP	*A*2, NADP	*B*, $P6_222$ empty	*C*, NAD	*D*, *C*2-empty
X-ray source	SRS, 9.5†	In house†	In house	In house	SRS, 9.6
Temperature	Room temperature	Room temperature	Room temperature	Room temperature	100 K
Wavelength (Å)	0.92	1.54	1.54	1.54	0.87
Resolution (Å)	28–2.8 (2.9–2.8)	25.0–2.16 (2.24–2.16)‡	21.0–2.4 (2.53–2.40)	20.0–2.47 (2.6–2.47)§	25.0–2.2 (2.3–2.2)
No. of reflections measured	43775 (2776)	93186 (7164)	115220 (18339)	45041 (3135)	57502 (4403)
No. unique	14948 (1335)	32868 (2822)	24902 (3523)	16682 (1406)	24710 (2148)
Redundancy¶	2.9 (2.1)	2.8 (2.5)	4.6 (5.2)	2.7 (2.2)	2.3 (2.0)
$I/\sigma(I)$	7.7 (2.5)	8.1 (1.8)‡	12.7 (3.7)	7.0 (1.6)§	12.6 (2.9)
R_{sym}†† (%)	10.8 (23.9)†	13.8 (50.6)†	11.3 (41.8)	10. 1 (48.0)	8.1 (29.8)
Completeness (%)	88.0 (80.2)	90.2 (81.3)	94.1 (93.0)	88.9 (81.7)	96.4 (85.2)

† R_{merge} between data sets *A*1 and *A*2 for terms where $I > 3\sigma(I)$ is 14.9%. The data sets were used individually and not merged. ‡ In the range 2.58–2.41 Å, $I/\sigma(I) = 2.4$. § In the range 2.76–2.60 Å, $I/\sigma(I) = 2.4$. ¶ Redundancy = average number of measurements for each reflection which contributed to the calculation of R_{sym}. †† $R_{sym} = \sum_{hkl} |\langle I_{hkl}\rangle - I_{hkl}|/\sum_{hkl}\langle I_{hkl}\rangle$, where $\langle I_{hkl}\rangle$ represents the average intensity of symmetry-equivalent reflections.

2.2. *L. mesenteroides* G6PD crystallized in $P6_222$

2.2.1. Crystallization. $NADP^+$-binding studies were carried out with G6PD mutant Q365C. Initial screens for possible crystallization conditions were carried out by hanging-drop vapour diffusion using Hampton Research Crystal Screens I and II (Jancarik & Kim, 1991). Refinement of the most promising conditions gave hexagonal pillars (*A*) (approximate dimensions 1.0 × 0.3 × 0.3 mm). Drops made by mixing 5 mg ml^{-1} Q365C in 100 m*M* Tris–HCl pH 7.5 and 500 µ*M* $NADP^+$ with an equal volume of well buffer were equilibrated for 3 months at 291 K against 1.64 *M* unbuffered ammonium sulfate. Crystals of the same habit (*B*) were grown from drops containing equal volumes of 5 mg ml^{-1} Q365C in 100 m*M* Tris–HCl pH 7.5 and 12.5 m*M* NAD^+ and well buffer. The final pH of the drops after equilibration with well buffer was close to 5.8. The space group for both sets of crystals was $P6_222$, with unit-cell parameters $a = b = 136.7$, $c = 121.2$ Å ($\alpha = \beta = 90$, $\gamma = 120^\circ$); there is one subunit in the asymmetric unit and a solvent content of 60%.

2.2.2. X-ray data collection. Two room-temperature data sets were collected for the $NADP^+$ binary complex; the first (*A*1), for an initial study at 2.8 Å resolution, was collected on station 9.5 at the CCLRC synchrotron-radiation source, Daresbury Laboratory. Once coenzyme binding had been confirmed, a second more complete data set was collected on a conventional source, collecting data to 2.2 Å (*A*2). A 2.4 Å room-temperature data set (*B*) for G6PD Q365C grown in this crystal form in the presence of NAD^+ was also collected. All three data sets were indexed, integrated, scaled and merged with the *HKL* program suite (Otwinowski & Minor, 1997). Data-collection statistics are given in Table 1; 8% of the terms were randomly selected for free *R*-factor validation and were not included in any refinement (Brünger, 1992*a*).

2.2.3. Molecular replacement. An *X-PLOR* rotation-function search (Brünger, 1992*b*) using the 2.8 Å data set *A*1 and a search model consisting of the well ordered subunit AP gave a peak 4.2σ above the next highest peak and 9.6σ greater than the mean. After Patterson correlation refinement, the correlation coefficient was 0.11 and the next highest solution (correlation coefficient 0.06) represented a similar orientation of the molecule. The remaining possible solutions had correlation coefficients of 0.025 or less. An *X-PLOR* translation-function search using the indicated orientation gave a single peak 7.5σ greater than the next highest peak. Following *X-PLOR* rigid-body refinement (Brünger, 1992*c*), the *R* and free *R* factors of the initial solution were 32.3 and 33.1%, respectively; Powell conjugate-gradient minimization reduced these to 22.6 and 32.1%, respectively.

2.2.4. Refinement and model building of $NADP^+$ complex. σ_A-weighted (Read, 1986) $2F_{obs} - F_{calc}$ and $F_{obs} - F_{calc}$ electron-density maps were generated using the *CCP*4 program suite (Collaborative Computational Project, Number 4, 1994). Difference density for $NADP^+$ was clearly visible in the expected nucleotide-binding site and it was also clear that the 2′-phosphate-binding residue Arg46 had changed orientation and become more ordered. Several cycles of manual rebuilding using *O* (Jones & Kjeldgaard, 1997) followed by *X-PLOR* (versions 3.1 and 3.851) energy minimization were carried out. Later cycles used data set *A*2, which extends to 2.2 Å resolution. Simulated-annealed maps which omitted contributions from $NADP^+$ were utilized to reduce phase bias. A bulk-solvent correction was applied to allow inclusion of low-resolution terms. Water molecules were included at stereochemically sensible positions in the structure where the electron density was at least 1σ in the $2F_{obs} - F_{calc}$ map and at least 3σ in the $F_{obs} - F_{calc}$ map.

The final model, referred to as 'NADP', contains all 485 G6PD residues, one $NADP^+$ molecule, one sulfate ion and 191 water molecules. At convergence, the *R* and free *R* factors are 18.7 and 22.6%, respectively and 89% of the residues lie within the most favoured regions of a Ramachandran plot, as defined by *PROCHECK* (Laskowski *et al.*, 1993). Refinement details and quality indicators are given in Table 2.

2.2.5. Attempt to bind NAD^+. A difference electron-density map using data set *B* and an initial model of the protein generated by rigid-body refinement using only protein atoms from the NADP structure showed NAD^+ was not bound in this

Table 2
Refinement statistics and quality indicators.

Values in parentheses refer to the highest resolution shell.

Data set	*A*, NADP	*B*, $P6_222$-empty	*C*, NAD	*D*, *C*2-empty
Resolution (Å)	30.00–2.16 (2.24–2.16)	30.00–2.40 (2.49–2.40)	20.00–2.47 (2.56–2.47)	25.00–2.20 (2.28–2.20)
Observations in refinement working set	30113 (2606)	22862 (2180)	15703 (904)	23512 (2043)
Observations in validation set	2572 (216)	2002 (206)	810 (46)	1198 (105)
R factor (%)	18.7 (31.6)	19.0 (28.3)	21.3 (32.2)	20.6 (31.7)
Free *R* factor	22.6 (32.3)	23.6 (35.6)	29.2 (36.6)†	28.2 (34.0)†
Mean *B*, main-chain atoms (Å^2)	29.8	31.6	27.7	24.0
Mean *B*, side-chain atoms (Å^2)	31.9	33.4	29.9	26.2
Mean *B*, waters (Å^2)	39.2	39.3	26.2	28.5
Mean *B*, coenzyme (Å^2)	38.5		49.0	
Mean coordinate error‡ (Å)	0.35	0.38	0.38	0.38
R.m.s.d. distances (Å)	0.006	0.006	0.006	0.005
R.m.s.d. bond angles (°)	1.26	1.27	1.26	1.24
Ramachandran plot§				
% Residues most favoured	89.3	89.1	87.0	90.4
% Additionally allowed	10.5	10.7	12.5	9.4
% Generously allowed	0.2	0.2	0.5	0
% Disallowed (residue No.)	0	0	0	0.2 (221)

† The relatively large difference (>7.5%) between *R* factor and free *R* factor for these data sets is likely to arise from the difficulty in describing the region 55–70 with a single conformation. ‡ As determined from the resolution dependence of σ_A (Read, 1986). § As defined by *PROCHECK* (Laskowski *et al.*, 1993).

crystal form. The structure was built and refined as above to provide a comparison of the conformation of the protein with and without $NADP^+$ in these crystallization conditions; it is referred to as '$P6_222$-empty'. The final model contains all protein residues, 139 water molecules and a sulfate ion. At convergence, the *R* and free *R* factors are 19.0 and 23.6%, respectively; 89.5% of the residues lie within the most favoured region of the Ramachandran plot. Quality indicators are again given in Table 2.

2.3. *L. mesenteroides* G6PD crystallized in *C*2

2.3.1. Crystallization. NAD^+-binding studies were carried out with G6PD mutant S215C. Initial screens for possible crystallization conditions were carried out by hanging-drop vapour diffusion using Hampton Research Crystal Screens I and II (Jancarik & Kim, 1991). A higher protein concentration was used than for previous trials. Refinement of the most promising conditions gave rectangular plates with approximate dimensions 0.7 × 0.3 × 0.05 mm. These crystals grew when protein drops were equilibrated for two weeks at 291 K against 20%(*v*/*v*) PEG 400 in 0.1 *M* HEPES–NaOH pH 7.5 containing 200 m*M* $CaCl_2$. The drops were made by mixing equal volumes of well buffer and a 10 mg ml^{-1} solution of S215C in 100 m*M* Tris–HCl pH 7.5 and 12.5 m*M* NAD^+. Initial diffraction studies identified the space group as *C*2, with unit-cell parameters a = 131.9, b = 45.2, c = 93.5 Å, $\alpha = \gamma = 90$, $\beta = 107.1^\circ$; there is one subunit in the asymmetric unit and a solvent content of 40%.

2.3.2. X-ray data collection. An initial 2.4 Å data set (*C*) was collected in-house at room temperature and processed using the *HKL* suite. The crystals could be flash-frozen without difficulty when soaked for 5 min in mother liquor containing 20% glycerol. A second data set (*D*) was therefore collected to 2.2 Å from a frozen crystal held in a stream of liquid nitrogen at 100 K provided by an Oxford Cryosystems Cryostream cooler (Garman & Schneider, 1997) on station 9.6 at the CCLRC synchrotron-radiation source, Daresbury Laboratory. This crystal had unit-cell parameters a = 129.3, b = 44.3, c = 91.2 Å, $\alpha = \gamma = 90$, $\beta = 105.4^\circ$. Table 1 gives statistics for both data sets; 5% of the terms were set aside for free *R*-factor validation.

2.3.3. Molecular replacement. A rotation and translation search was carried out for each data set independently using the *AMoRe* (Navaza, 1994) and *TFFC* (Tickle, 1992) programs available with the *CCP*4 suite and, as for the $NADP^+$ complex, the AP subunit as a model. The best rotation-function solution used normalized structure factors from data set *C* and had a peak height of 49.6, the next highest peak being 17.4. The peak height of the best solution from *D* was 48.8, with a next highest peak of 16.1. Translation searches using the indicated orientations gave a solution for *C* at a height of 6.00 with a signal-to-noise ratio of 24.9 and a solution for *D* at 6.47 with a signal-to-noise ratio of 26.7. After a round of *X-PLOR* rigid-body minimization, the *R* and free *R* factors were 35.2 and 35.7%, respectively, for data set *C* and 36.7 and 38.8%, respectively, for *D*.

2.3.4. Refinement. The initial $2F_{obs} - F_{calc}$ and $F_{obs} - F_{calc}$ electron-density maps showed no connected density for NAD^+ with either data set. However, a region of the polypeptide chain close to the coenzyme-binding region (residues 55–70) had only poor density and required extensive rebuilding. Several rounds of manual building using *O* and minimization by *X-PLOR*, utilizing both conjugate-gradient minimization and simulated-annealing omit maps, were carried out against data set *D*, whose higher resolution aided interpretation. It became clear that NAD^+ was not bound to G6PD in the crystal which had been frozen. Inspection of the nucleotide-binding region in maps calculated from data set *C* with the improved protein model revealed that NAD^+ had bound at room temperature. Both the NAD^+-bound structure, referred to as 'NAD', and the unliganded structure, referred to as '*C*2-empty', were refined using a procedure similar to that for the $NADP^+$ binary complex. A bulk-solvent correction was used in both refinements.

At convergence, the *R* and free *R* factors were 21.3 and 29.2%, respectively, for the data from set *C* between 20.0 and 2.47 Å, and 20.6 and 28.2%, respectively, for the data from set *D* between 25.0 and 2.2 Å. Refinement parameters for the two structures are given in Table 2. Both models contain all 485

residues of the G6PD monomer. In addition, the NAD structure contains one NAD^+ and 61 water molecules and the *C*2-empty structure contains 188 water molecules, a calcium ion and one glycerol molecule (the cryoprotectant). 87% of the residues in the NAD complex and 90% in the *C*2-empty model are in the most favoured regions of the Ramachandran plot.

2.4. Ternary complex of D177N G6PD with NADPH and G6P

Crystallization, X-ray data collection, solution and refinement of this structure are described elsewhere (Cosgrove *et al.*, 2000). Crystals were grown under similar conditions to those described for the NAD^+ complex. The space group is *C*2, with unit-cell parameters (at 100 K) $a = 129.0$, $b = 44.0$, $c = 91.1$ Å, $\alpha = \gamma = 90$, $\beta = 105.2^\circ$. After refinement at 2.48 Å resolution, the final *R* and free *R* factors for this complex were 20.5 and 29.6%, respectively.

3. Results

3.1. $NADP^+$-bound and unliganded structures in $P6_222$

Crystals of the G6PD mutant Q365C which grew in space group $P6_222$ from unbuffered ammonium sulfate (pH 5.8) in the presence of $NADP^+$ were found to contain bound coenzyme. There is a monomer in the asymmetric unit; the two subunits of the dimer are identical and related by a crystallographic twofold axis parallel to the *ab* plane.[1]

As in the G6PD-P structure (Rowland *et al.*, 1994), residues 221–226 and 293–298 form surface loops and have higher than average temperature factors; some side chains of these residues are not ordered. In this binary complex, the atoms of the coenzyme domain have very similar temperature factors to those of the $\beta + \alpha$ domain; the mean temperature factors ($B_{\rm mean}$) for all atoms in each domain are 31.6 and 30.4 $Å^2$, respectively. In contrast, even in the better ordered AP subunit of the enzyme crystallized from phosphate, the corresponding temperature factors were 36.1 and 30.1 $Å^2$, respectively. The final $2F_{\rm obs} - F_{\rm calc}$ electron-density map in the region of $NADP^+$ is shown in Fig. 1 together with that for a difference map in which the coenzyme was omitted from $F_{\rm calc}$. The nicotinamide ring is less ordered than the remainder of the coenzyme and not all of its atoms are clearly visible in the final density. The occupancy of the coenzyme was reduced to 0.75 during refinement in order to match the temperature factors of the dinucleotide to those of its protein ligands.

Electron-density maps for G6PD Q365C crystallized from ammonium sulfate in the presence of 12.5 m*M* NAD^+ showed that NAD^+ would not bind in this space group under the conditions investigated. Despite the absence of bound coenzyme, the coenzyme-binding domain of this 'empty' structure remains relatively well ordered. Values of $B_{\rm mean}$ for the two domains are 34.0 and 31.6 $Å^2$. Both Arg46 and Gln47 are less well ordered than in the $NADP^+$ complex. The r.m.s. difference in the coordinates of main-chain atoms between the NADP and $P6_222$-empty structures when optimally superimposed is small (0.18 Å).

3.2. NAD^+-bound and unliganded structures in *C*2

Crystals of the G6PD mutant S215C grew from PEG 400 in HEPES/$CaCl_2$ at pH 7.5 in the space group *C*2 with a monomer in the asymmetric unit; the two subunits of the dimer are again related by a crystallographic twofold axis and are therefore identical. NAD^+ was bound to the protein in the crystal for which data was collected at room temperature (data set *C*). The occupancy of the NAD coenzyme was reduced to 0.6 during refinement in order to match the temperature factors of the dinucleotide to those of its protein ligands. The electron density in the region of the coenzyme in the final refined $2F_{\rm obs} - F_{\rm calc}$ map, together with difference electron density in which the coenzyme was omitted from $F_{\rm calc}$, is shown in Fig. 2. The nicotinamide ring is again disordered; breaks in the $2F_{\rm obs} - F_{\rm calc}$ density close to the adenine ribose also indicate some disorder. The breaks are less severe in the difference map; they suggest both flexibility of this ribose and small differences in the protein conformation between the 60% of molecules with bound coenzyme and the 40% without.

When data for this crystal form were collected at 100 K (data set *D*), NAD^+ was not bound. In both the NAD and *C*2-empty structures all 485 residues are visible in the electron-density maps and prolines 149 and 375 again have the *cis* conformation. Again, the most disordered parts of the protein include the two large surface loops, residues 221–226 and 293–298. The loop between helix αb and helix αb′ is also disordered, while helix αb itself shows some mobility in the NAD structure. The calcium ion and glycerol molecule found in the 100 K *C*2-empty structure are bound between molecules. The r.m.s. difference in main-chain coordinates between the NAD and *C*2-empty structures is 0.44 Å.

3.3. The NADPH–G6P complex of D177N G6PD in space group *C*2

In the abortive ternary complex of this low-activity mutant, the substrate G6P and the adenine nucleotide of NADPH can be seen in difference electron-density maps. The G6P phosphate binds at the 'outer' phosphate site. Details and implications of substrate binding in this complex have been discussed elsewhere (Cosgrove *et al.*, 2000). The density in the region of coenzyme in the final $2F_{\rm obs} - F_{\rm calc}$ map and in a difference map in which the coenzyme has been omitted from $F_{\rm calc}$ are shown in Fig. 3. In this map the density for the adenine, 2′-phosphate, adenine ribose and 5′-phosphate moieties are clear. There is fragmentary non-continuous density which may correspond to parts of the nicotinamide nucleotide. During refinement, only the adenine nucleotide was included in the model and its occupancy was reduced to 0.75. The regions of the G6PD molecule which are disordered in this complex are the same as in the NAD structure and the

[1] The subunit deposited in the PDB forms a dimer by rotation about the axis parallel to [110] at height 1/3.

*C*2-empty structure. A calcium ion is bound between molecules as in the *C*2-empty structure.

3.4. Binding sites

3.4.1. NADP$^+$. NADP$^+$ is shown in its binding site in the protein in Fig. 4(*a*); the convention used for labelling the atoms of each coenzyme is given in Fig. 4(*d*). The bound NADP$^+$ is open with the adenine ring in the *anti* conformation; the nicotinamide ring has been built *syn*. Potential hydrogen bonds and non-polar contacts are listed in Table 3. NADP$^+$ binds, as anticipated, with the two ribose rings and the bis-phosphate straddling the C-termini of the parallel sheet strands of the coenzyme domain. There are hydrogen bonds from the adenine ribose 3′-hydroxyl and the bis-phosphate O atoms to the main-chain N atoms of Gly15, Asp16 and Leu17 of the nucleotide-binding fingerprint in the βA–αa turn. The nicotinamide ribose contacts residues of the βD–αd tight turn (117–120) and the βE–αe turn (147–153).

There is an important interaction between Arg46 and the 2′-phosphate, with hydrogen bonds made by both N$^{\varepsilon}$ and N$^{\eta2}$ of the arginine to two phosphate O atoms. The third phosphate O atom makes a hydrogen bond to an ordered water which is hydrogen bonded itself to Thr14 O$^{\gamma1}$ and Gln47 N$^{\varepsilon2}$. Thr14 O$^{\gamma1}$ makes a further hydrogen bond to the adenine ribose 3′-hydroxyl.

The adenine ring is sandwiched between Arg46 and the residues His84, Asp85 and Val86 of the βC–αc loop. There is a plane-to-plane π–π contact between the adenine and the guanidinium group of this arginine. A hydrogen bond is possible between Asp85 O$^{\delta1}$ and the amino substituent of the adenine ring. There are few contacts to the nicotinamide; the ring is oriented with the *Si* face towards the predicted active site. The nicotinamide amide contacts Asp16 O$^{\delta2}$ and also makes a hydrogen bond to an O atom of the nicotinamide phosphate. Three further interactions are mediated through waters, as noted in Table 3.

3.4.2. NADPH. The binding site for NADPH is shown in Fig. 4(*b*); only the adenosine nucleotide, which is reasonably well defined in this ternary complex, has been built. Contacts between the dinucleotide fingerprint and the adenosine moiety of NADPH are similar to those for NADP$^+$ (Table 3): O3′ of the adenine ribose again interacts with Gly15 main-chain N atom and with Thr14 O$^{\gamma1}$, while the 5′-phosphate interacts with the main-chain N atom of Asp16. A similar but not identical pattern of contacts occurs for the 2′-phosphate; it interacts with Arg46 N$^{\eta2}$ and the main-chain N atoms of 46 and 47. Gln47 N$^{\varepsilon2}$, although it is not completely ordered, can also make a direct contact with the 2′-phosphate, but the side-chain orientation of Arg46 complements the NADPH 2′-phosphate less well than it did that of NADP$^+$. The π–π contact between Arg46 and the adenine ring is again present, as is the interaction with O$^{\delta1}$ of Asp85. The adenine ring in this complex also interacts with Phe122; longer distances are observed for the NADP$^+$ complex. While the fragmentary density which may correspond to the nicotinamide nucleotide would suggest a different coenzyme conformation in the NADPH–G6P complex, the obvious and possibly more

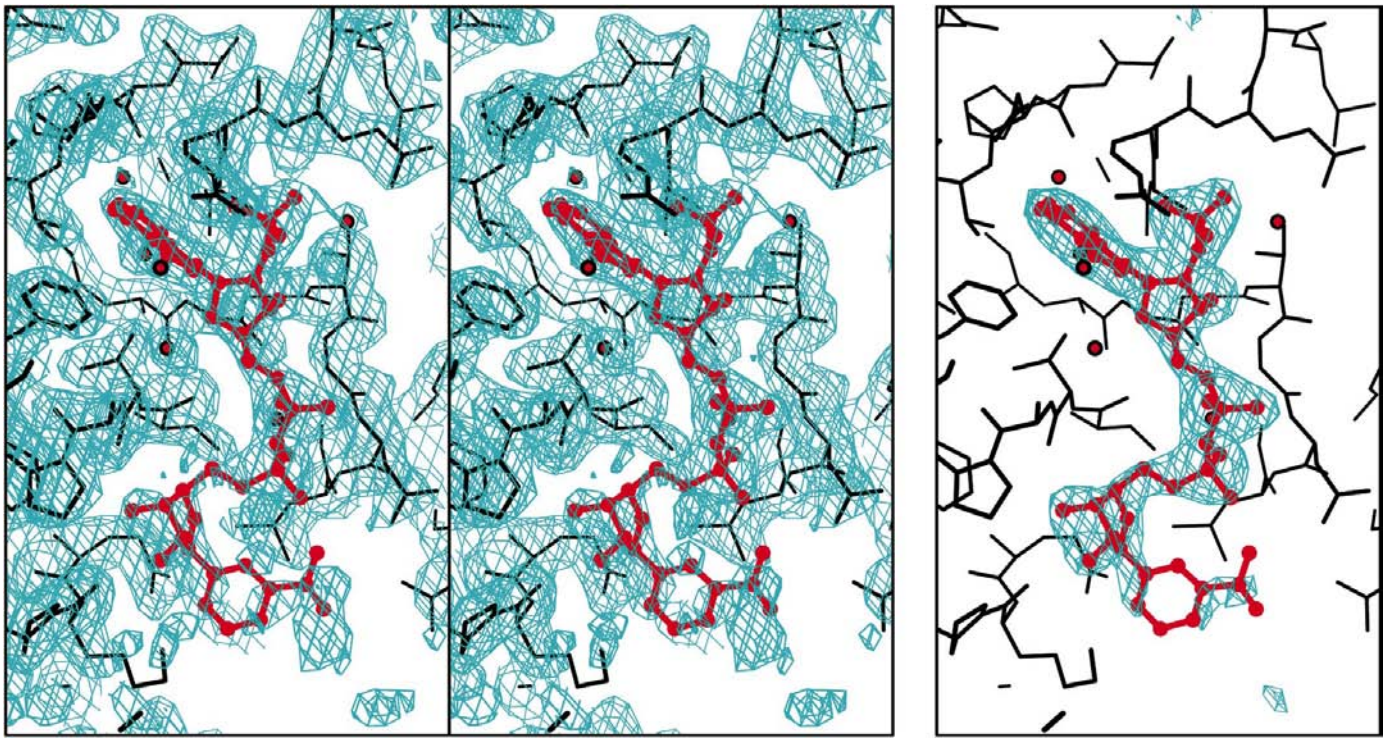

Figure 1
Stereo image of the final $2F_{obs} - F_{calc}$ electron-density map of the NADP$^+$ complex, crystallized in $P6_222$, in the region of the NADP$^+$ site, contoured at 1σ. Difference electron density with NADP$^+$ omitted from F_{calc}, contoured at 4σ. This and subsequent figures have been drawn using the programs *Bobscript* (Esnouf, 1997; an extension of *Molscript*; Kraulis, 1991) and *Render* (Bacon & Anderson, 1988; Merritt & Murphy, 1994).

significant feature is that this part of the reduced nucleotide in this inactive ternary complex is not ordered.

3.4.3. NAD$^+$. NAD$^+$ is shown in its binding site in Fig. 4(*c*). The coenzyme is in a similar but not identical conformation to NADP$^+$, with the adenine ring again *anti* (the nicotinamide ring is not localized). Contacts are given in Table 3. NAD$^+$ binds across the sheet as does NADP$^+$; there are again hydrogen bonds from the bis-phosphate to the first turn of helix αa. As expected, there are specific differences in the contacts of the adenine ribose; there are small but significant differences throughout the binding site. The most obvious feature of NAD$^+$ binding is the poorer order in the binding site than that found for NADP$^+$.

While the main-chain N atom of Arg46 interacts with the adenine ribose 2′-hydroxyl, the side chain is disordered. The 2′-hydroxyl is hydrogen bonded by Gln47 O$^{\varepsilon1}$. As in the NADP and NADPH–G6P structures, the adenine ribose 3′-hydroxyl makes a hydrogen bond to Thr14 O$^{\gamma1}$. The nicotinamide phosphate of NAD$^+$ makes a direct contact to the Asp16 main-chain N atom; this N atom hydrogen bonds both adenine and nicotinamide phosphate of NADP$^+$ and the adenine phosphate of NADPH. A direct contact to Ser117 O$^{\gamma}$ is seen only with NAD$^+$. There is again a hydrogen bond between the main-chain carbonyl of Lys148 and the 2′-hydroxyl of the nicotinamide ribose. In the electron-density map the nicotinamide ribose and its phosphate are the best ordered part of NAD$^+$.

Since Arg46 is not well ordered in the absence of a 2′-phosphate, it does not stabilize the adenine ring by a π–π interaction. The contacts between the adenine and Asp85 and Val86 are also weaker. Although the adenine ring is a little closer to Phe122 than in the NADP$^+$ complex, the adenine site is less well defined. The adenine and adenine ribose are clearly not as tightly bound or as well ordered as in either the NADP$^+$ binary complex or the NADPH–G6P ternary complex.

3.4.4. Sulfate and calcium ions. Both the NADP and $P6_222$-empty structures have one sulfate ion bound to the protein. This site is essentially that of the 6-phosphate of bound G6P in both the NADPH–G6P complex and the G6P binary complex (Cosgrove *et al.*, 2000) and of the 'outer' phosphate in subunit AP of G6PD-P (Rowland *et al.*, 1994). The same contacts are made in all complexes: to His178 N$^{\varepsilon2}$, Tyr179 O$^{\eta}$ and Lys182 N$^{\zeta}$, all in the conserved eight-residue peptide, and to Lys343 N$^{\zeta}$; this residue is lysine or arginine in most of the known sequences. With no simple oxoacid anion present in the crystallization buffer or precipitant for the *C*2 NAD$^+$ binary or *C*2-empty structures, no anion interacts with His178.

In the *C*2-empty structure and in the NADPH–G6P ternary complex, a calcium ion binds at a position linking symmetry-related molecules. While the concentration of calcium ions was high in the precipitant for this crystal form and it is known to inhibit the enzyme (unpublished results), the ion did not bind in the room-temperature NAD$^+$ complex. In the *C*2-empty structure there are seven calcium contacts: to Asn477 O$^{\delta1}$, to two hydroxyls of a molecule of the cryoprotectant (glycerol) and to four waters. One of the water molecules is bound to Glu319 O$^{\varepsilon2}$. Waters in the second coordination sphere bridge the glycerol and the calcium ion to

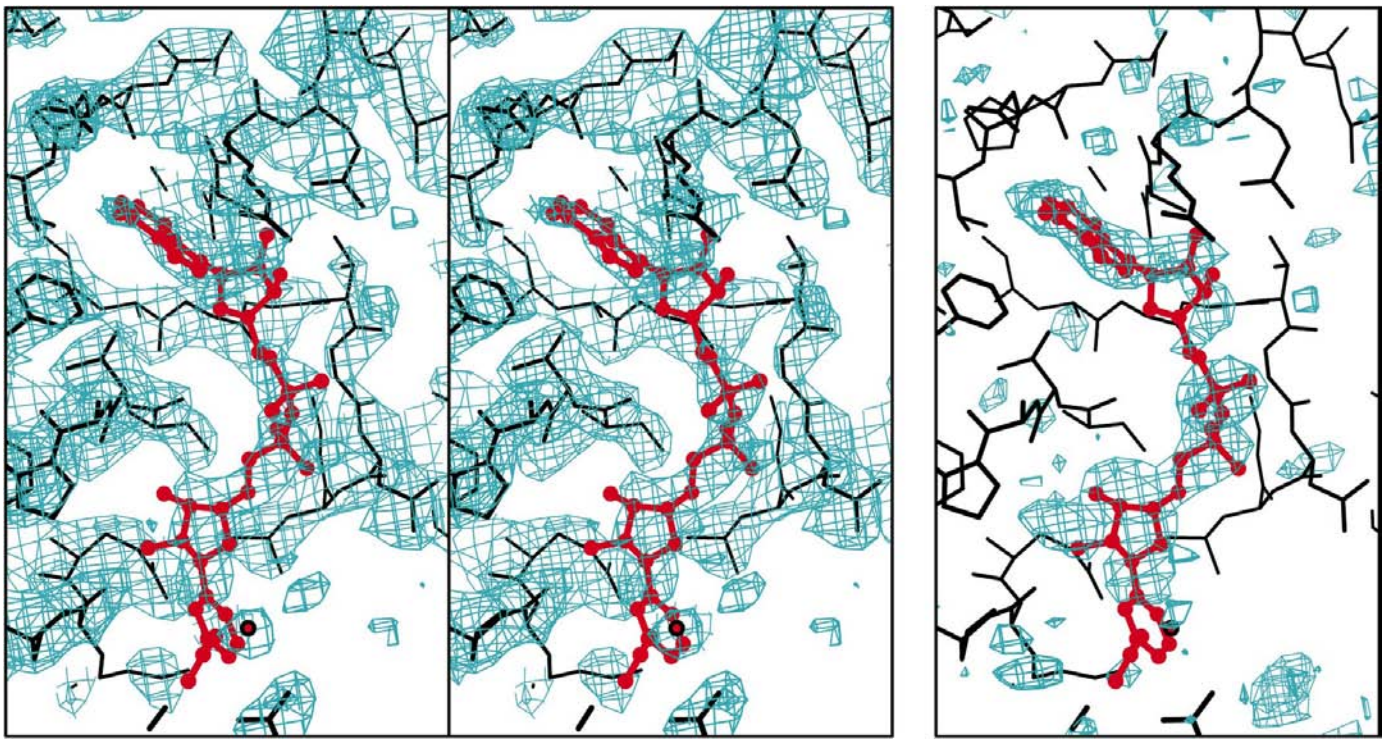

Figure 2
Stereo image of the final $2F_{obs} - F_{calc}$ electron-density map of the NAD$^+$ complex, crystallized in *C*2, in the region of the NAD$^+$ site, contoured at 1σ. Difference electron density with NAD$^+$ omitted from F_{calc}, contoured at 2.5σ.

Glu101 of a symmetry-related dimer. None of these residues is conserved. A similar arrangement is found in the ternary complex structure and in the structure of the D177N enzyme grown with NAD^+ but with only minimal NAD^+ bound ('D177N-nad'; Cosgrove *et al.*, 2000). The details differ since the glycerol has been modelled by two waters in these structures. The calcium is distant from both the coenzyme and the substrate site. The cryoprotectant appears to be necessary to complete the coordination sphere of the calcium ion; there is no evidence of an ordered metal ion in the room-temperature NAD^+ binary structure.

Table 3
Coenzyme protein contacts.

(*a*) Potential hydrogen bonds (Å). Distances greater than 3.5 Å are given (in parentheses) for comparison between structures. The water–nicotinamide NAD^+ interaction is in parentheses since the nicotinamide ring is not localized.

Coenzyme moiety	Protein residue	No.	Secondary structure	Atom	$NADP^+$ distance	NADPH distance	NAD^+ distance
Adenine							
N3A	Water	1040†		O	2.98		
N1A	Val	86	βC–αc	N	3.03	3.20	(3.54)
N7A	Water	1231†		O	2.85		
N6A	Asp	85	βC–αc	$O^{\delta1(2)}$	3.44	2.99	(3.57)
Adenine ribose							
O4R	Water	1162†		O	2.96		
O3R	Gly	12	βA–αa	O	3.50	3.48	
	Thr	14	βA–αa	$O^{\gamma1}$	2.75	2.70	2.57
				N	3.44	3.49	3.47
	Gly	15	βA–αa	N	2.98	3.15	(3.95)
O2R	Thr	14	βA–αa	$O^{\gamma1}$	3.29	3.38	
	Arg	46	βB–αb	N			3.46
	Gln	47	βB–αb	$O^{\varepsilon1}$			2.82
	Water	1210†		O	3.41		
2′-phosphate							
O1P	Arg	46	βB–αb	$N^{\eta2}$	2.74	3.26	
O2P	Arg	46	βB–αb	N	2.86	2.52	
				N^{ε}	2.79	(3.62)	
	Gln	47	βB–αb	N		2.74	
O3P	Thr	14	βA–αa	$O^{\gamma1}$	(3.87)	3.04	
	Gln	47	βB–αb	N	3.06	(3.91)	
				$N^{\varepsilon2}$		3.27	
	Water	1210†		O	2.48		
Bis-phosphate							
O2A	Asp	16	αa	N	3.30	2.81	
O3	Asp	16	αa	N			3.36
O1N	Asp	16	αa	N			2.72
	Leu	17	αa	N	(3.81)		2.77
O2N	Asp	16	αa	N	3.31		3.40
	Leu	17	αa	N	2.86		(3.65)
	Ser	117	βD–αd	O^{γ}	(3.92)		3.29
	Water	1192†		O	2.57		
Nicotinamide ribose							
O3Q	Val	118	βD–αd	O	2.78		(3.73)
O2Q	Lys	148	βE–αe	O	2.93		2.46
Nicotinamide							
N7N	Asp	16	αa	$O^{\delta2}$	3.32		
	(Water	674†					2.63)

4. Discussion

4.1. Changes in protein conformation in different complexes and crystal forms

In all the structures reported in this paper, the G6PD dimer consists of two identical subunits related by a crystallographic twofold axis. This differentiates all five from the structure of the apoenzyme crystallized from phosphate, in which the two subunits differ in conformation. All subunits resemble subunit AP in containing a *cis* Pro149. Superposition of the NADP structure onto subunit AP gives an r.m.s. deviation in the position of all main-chain atoms of 0.70 Å. The coenzyme and $\beta + \alpha$ domains can be superimposed individually with r.m.s. deviations of 0.48 and 0.35 Å, respectively. The better superposition of the individual domains suggests an overall change in the relationship between them and in interdomain contacts.

Evidence for domain movement is reinforced if the mean differences for all main-chain atoms are compared for all structures with the $\beta + \alpha$ domains optimally aligned (Table 4). The small differences between all $\beta + \alpha$ domains suggest that the intersubunit contacts are unchanged from those seen in G6P-P for all the structures described here and this is confirmed by inspection of the interface. The $P6_222$-empty structure is essentially the same as the NADP structure crystallized in the same space group and will not be discussed further. On this alignment, the coenzyme-binding domains differ most between NADP and subunit BP, with *trans* Pro149. Subunit AP, the *C*2-empty structure and the ternary complex structures are similar to one another but different from NADP. The NAD and *C*2-empty structures differ in the relation between their domains; the NAD structure appears to be intermediate between the NADP and AP structures. The D177N-nad structure determined at 100 K (Cosgrove *et al.*, 2000) is similar to the NAD structure: the mean overall scalar difference is 0.37 Å and the resultant vector difference for the small domains when the $\beta + \alpha$ domains are aligned is 0.17 Å. The different orientations of the two domains with respect to each other can be seen in Fig. 5, where the small domains of nine different subunits are superposed. The movement of the NADP structure relative to that of subunit AP results in an opening of the active-site cleft and a slight closing of the opposite end of the interdomain surface. The active-site cleft in subunit BP is most tightly closed.

The most concerted movement within the small domains of the NADP and NAD structures relative to that of subunit AP is that of the sheet residues. The direction of the resultant vector is within 20° of the sheet plane; movement in this

Table 3 (continued)

(*b*) C—C, C—N, C—O contacts 3.0–4.0 Å. Distances greater than 3.5 Å are in parentheses.

Coenzyme moiety	Residue	No.	$NADP^+$	NADPH	NAD^+
Adenine					
	Ala	45	(C^{α})	(C^{α})	(C^{α}), (C)
	Arg	46	C^{ζ}, (C^{γ}), (C^{δ}), (N^{ε}), ($N^{\eta 1}$)	C^{γ}, (N), (C^{δ}), (N^{ε}), (C^{ζ})	
	His	84	O	O, (C^{α}), (C), ($O^{\delta 2}$)	O
	Asp	85	(C^{α}), (C)		(C^{α}), ($O^{\delta 2}$)
	Val	86	$C^{\gamma 1}$, $C^{\gamma 2}$, (C^{α}), (C^{β})	$C^{\gamma 2}$, (C^{β}), ($C^{\gamma 1}$)	(N), ($C^{\gamma 1}$), ($C^{\gamma 2}$)
	Phe	122	(C^{ζ})	$C^{\varepsilon 2}$, C^{ζ}, ($C^{\varepsilon 1}$)	(C^{ζ})
Adenine ribose					
	Gly	12	C^{α}, C	C^{α}, C	C^{α}, (C), (O)
	Thr	14	C	(C^{α}), (C), (C^{β})	C^{β}, (C^{α}), ($C^{\gamma 2}$)
	Gly	15	(C^{α})	C^{α}	(N), (C^{α})
	Ala	45	C^{β}	C^{β}, (C^{α})	C^{β}
	Arg	46			C^{γ}
	Gln	47			(C^{δ})
	Ser	117			(O)
2′-phosphate					
	Ala	45	(C^{β}), (C)	C^{β}, C, (C^{α})	
	Arg	46	C^{β}, C^{γ}, C^{ζ}, (C^{α}), (C^{β})	C^{α}, C^{β}, C, (C^{γ}), (C^{ζ})	
	Gln	47	C^{β}, (C^{α})	C^{β}, (C^{α})	
Bis-phosphate					
	Gly	15	(C^{α}), (C)	C^{α}, (C)	C^{α}, C
	Asp	16	(C^{α}), (C), (C^{β})	C^{β}, (C^{α})	C^{α}, C^{β}, C
	Leu	17	C^{β}, (N), (C^{α})		(N), (C^{α}), (C^{β})
Nicotinamide ribose					
	Leu	17	($C^{\delta 2}$)		
	Ser	117	O, (C), (O^{γ})		(C)
	Val	118	(N), (C)		
	Glu	147	C^{γ}, $O^{\varepsilon 2}$, (C^{β}), (C^{δ})		C^{γ}, $O^{\varepsilon 1}$
Nicotinamide					
	Leu	17	C^{β}, (C^{α}), ($C^{\delta 1}$)		
	Glu	147	$O^{\varepsilon 2}$		$O^{\varepsilon 1}$
	Lys	148	(C^{γ}), (N^{ζ})		(C^{ε}), (N^{ζ})

† Potential hydrogen bonds involving water (Å) $NADP^+$ N3A–water 1040–Gly12 N 2.76; Thr44 O 3.33; water 1164 3.27; $NADP^+$ N7A–water 1231–Arg46 $N^{\eta 1}$ 3.20; $NADP^+$ O4R–water 1162–Ala119 N 2.89; $NADP^+$ O3P–water 1210–Thr14 $O^{\gamma 1}$ 2.65, Gln47 $N^{\varepsilon 2}$ 2.58; $NADP^+$ O2N–water 1192–Gly12 O 3.17, Leu17 N 3.39, Ala18 N 2.95, Ser117 O^{γ} 2.76 (NAD^+ N7N–water 674–Arg223 $N^{\eta 1}$ 3.22).

direction increases linearly with distance from Arg175. The movement may be described as a rotation about an axis approximately perpendicular to the sheet and passing through a point close to Arg175. The angle of rotation in the NADP structure is 5°; in the NAD structure there is a smaller rotation of approximately 2°. Although in both structures the movement of the rest of the domain is coupled to that of the sheet, it is more complex than a simple rotation and less well correlated with the distance from Arg175.

4.2. Implications for coenzyme specificity

The results described in this paper suggest that the hinge angle between the two domains of G6PD can vary between a relatively closed structure, exemplified by *C*2-empty, and a relatively open one, such as $P6_222$-empty. While the adenine nucleotide of $NADP^+$ and NADPH binds to either, the small changes in the main-chain atoms of the βB–αb turn on hinge opening enable the conserved Arg46 to be optimally oriented and best ordered in the open form. Interaction with this residue is crucial for binding the 2′-phosphate of $NADP^+$. Its importance has been shown by site-directed mutagenesis (Levy *et al.*, 1996); the mutants R46Q and R46A have K_m for $NADP^+$ enhanced 100-fold and 700-fold, respectively, with no more than a fourfold increase of K_m for the substrate G6P.

Other interactions with the adenine nucleotide have smaller importance as judged by K_m. A hydrogen bond is made between Thr14 $O^{\gamma 1}$ and the 3′-hydroxyl of the adenine ribose; mutation of this residue to alanine enhances K_m for $NADP^+$ tenfold (Vought *et al.*, 2000). Gln47, unique to the *L. mesenteroides* enzyme, makes different contacts in the closed and open structures: direct to the reduced coenzyme and through solvent to the oxidized coenzyme. The contact is unlikely to be energetically important since the mutant Q47A has a K_m for $NADP^+$ similar to that of wild-type enzyme (Vought *et al.*, 2000). The main-chain conformation of the dinucleotide-binding fingerprint is clearly important in orienting the bis-phosphate. The small change in conformation of these residues on closing the hinge angle is likely to contribute to disorder in the nicotinamide nucleotide of NADPH.

Since the coenzyme-binding site is at the edge of the extended G6PD dimer, residues important for binding are always close to crystal contacts. It is necessarily difficult to separate out the significance of different crystallization conditions in discussing the small changes of domain orientation. It is, for instance, possible that crystal contacts in the space group $P6_222$, which affect the βB–αb turn, αb, βC, the βc–αc turn and αc, will prevent the hinge angle closing. These studies, however, show that the open form of the molecule is of low enough free energy relative to that of the closed form that it can be stabilized by lattice forces in the absence of coenzyme. NAD^+ will not bind to this open form of G6PD grown from ammonium sulfate. The possibility of sulfate binding to a coenzyme phosphate site and competing with NAD^+ cannot be ruled out, although no sulfate ions are seen at the $NADP^+$ site in $P6_222$-empty G6PD. The more likely explanation is that the open conformation of the enzyme, which optimizes interaction with the coenzyme 2′-phosphate, is not optimal in supplying suitable residues to interact with the 2′-hydroxyl of NAD^+.

G6PD crystallized in space group *C*2 and described in this paper is either 'closed', when it may be unliganded or in a complex containing G6P, or 'half-open' with NAD^+ bound. The NAD structure was determined at room temperature but

the similar 'half-open' structure seen for D177N-nad was determined at 100 K. Hinge closing is therefore not likely to be a necessary consequence of flash-freezing. If the coenzyme domains of the NAD and *C*2-empty structures are superimposed, the coenzyme clashes with the 'closed' positions of Thr14, Ala45, Arg46 and Lys148. In the 'half-open' conformation these clashes are alleviated. Clashes also occur with Thr14 and Leu17 between NAD^+ and the furthest open form of G6PD; the small conformation differences of the fingerprint region as the coenzyme domains move make a significant difference to NAD^+/$NADP^+$ selectivity.

In the NAD^+ complex, the 2′-hydroxyl of the adenine ribose makes a hydrogen bond with Gln47 $O^{\varepsilon 1}$ and the 3′-hydroxyl with Thr14 $O^{\gamma 1}$. The Thr14 interaction, common to all complexes, contributes more to the catalytic efficiency of the NAD^+ reaction than of the $NADP^+$ reaction (Vought *et al.*, 2000). In most G6PD sequences this residue is serine, though threonine and, in two species, lysine are also found. In most species, the position equivalent to Gln47 is serine, alanine or threonine. The Gln47–NAD^+ contact may well be important in orienting NAD^+ but it is unlikely to contribute significantly to binding energy; the K_m for NAD^+ of the mutant Q47A is enhanced less than twofold (Vought *et al.*, 2000). While the interaction with Ser117 $O^{\gamma 1}$ is mediated by water in the $NADP^+$ complex, it is direct in the NAD^+ complex and this difference may contribute to the slightly different positions of NAD^+ and $NADP^+$ in the binding site (Fig. 4). This residue is either serine or alanine in the known sequences; alanine is more common.

Despite the fact that a glycine as the second residue of the nucleotide-binding fingerprint is unique to the *L. mesenteroides* enzyme, there are no direct contacts from it to either coenzyme, nor has mutation to alanine or serine affected coenzyme specificity (Vought & Levy, unpublished data). The φ,ψ dihedral angles of Gly13 are in the more restricted ranges allowed for any residue, close to those for an α-helix. In the 'half-open' conformation of the enzyme the rotation of the sheet provides features necessary to bind NAD^+. Small changes provide the correct orientation of the fingerprint residues in the tight βA–αa turn to optimize hydrogen bonds from main-chain atoms. The conformation of the βB–αb turn allows both Gln47 to interact correctly with the 2′-hydroxyl and Arg46 to be displaced from the position occupied by the adenine ring of NAD^+.

The low occupancy of NAD^+ and the poor surrounding density suggest there may be two closely related conformations of regions of the protein making contact with the coenzyme. Protein movement is required to make contacts between the adenine ribose and side chains of both Thr14 and Gln47 and also to avoid some unfavourable close contacts. While this movement optimizes interaction with the adenine ribose, it also serves to diminish contacts with the adenine ring. The side chain of Arg46 is no longer oriented to interact with the adenine ring, which is therefore exposed. In the less well tailored site, the adenine of NAD^+ does not approach residues 84–86 of the βC–αc loop as closely as does $NADP^+$ nor does it approach Phe122 as closely as does NADPH.

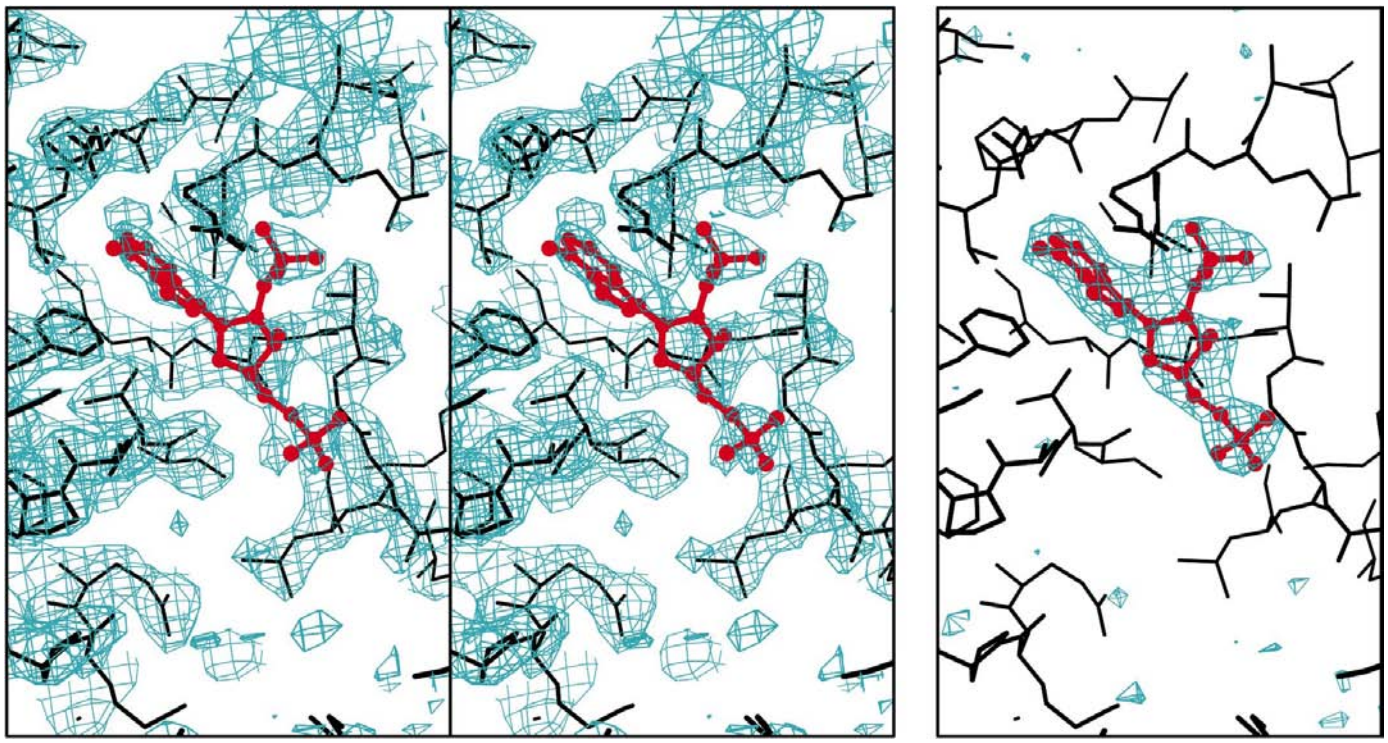

Figure 3
Stereo image of the final $2F_{obs} - F_{calc}$ electron-density map of the NADPH-G6P ternary complex, crystallized in *C*2, in the region of the NADPH site, contoured at 1σ. Difference electron density with coenzyme omitted from F_{calc}, contoured at 3σ.

Tighter binding of $NADP^+$ than NAD^+ is readily explained by the multiple roles of Arg46. While Thr14 and Gln47 are likely to make contributions to dual specificity of the enzyme of this species, the fit of the adenine ring as well as the ribose is clearly important. Except for Arg46, the residues forming the adenine pocket [the βC–αc loop (84–87) and the beginning of αd (121–123)] are poorly conserved; changes in this region will have a proportionately greater effect for NAD^+ than for $NADP^+$ binding.

The large K_d/K_m ratio for NAD^+ and the differing kinetic mechanisms for the NAD^+- and $NADP^+$-linked reactions have been cited as evidence that a change in enzyme conformation is required for productive NAD^+ binding (Haghighi & Levy, 1982; Levy, 1989). The relationship of the structures described here to that predicted conformation change is less clear. While it is tempting to equate it to the partial closing of the hinge angle and the reorientation of Arg46 and Gln47, the protein fluorescence change associated with NAD^+ binding is large and a greater conformation change was anticipated (Haghighi & Levy, 1982). Small differences in the conformations of the coenzymes themselves can be seen in Fig. 4; differences were also indicated in the nuclear Overhauser study (Levy, Ejchart *et al.*, 1983). Unfortunately, they are difficult to correlate since the solution experiments suggested changes at the nicotinamide ring, which is not well ordered in either complex in the crystal. It is necessary to consider the relationship of the coenzyme and substrate sites before further suggestions concerning the conformation change can be made.

In the NADPH–G6P ternary complex, G6P is bound in a suitable orientation for proton transfer from its β-1-hydoxyl to the catalytic base His240 (Cosgrove *et al.*, 2000). The nicotinamide nucleotide, however, is not ordered and this may represent the unproductive complex where G6P has bound first and closed the enzyme. This study may indicate that $NADP^+$, with tight binding at the adenine nucleotide, must first bind to the open form if the nicotinamide ring is ultimately to be oriented correctly. The further conformation change on binding substrate may then orient the

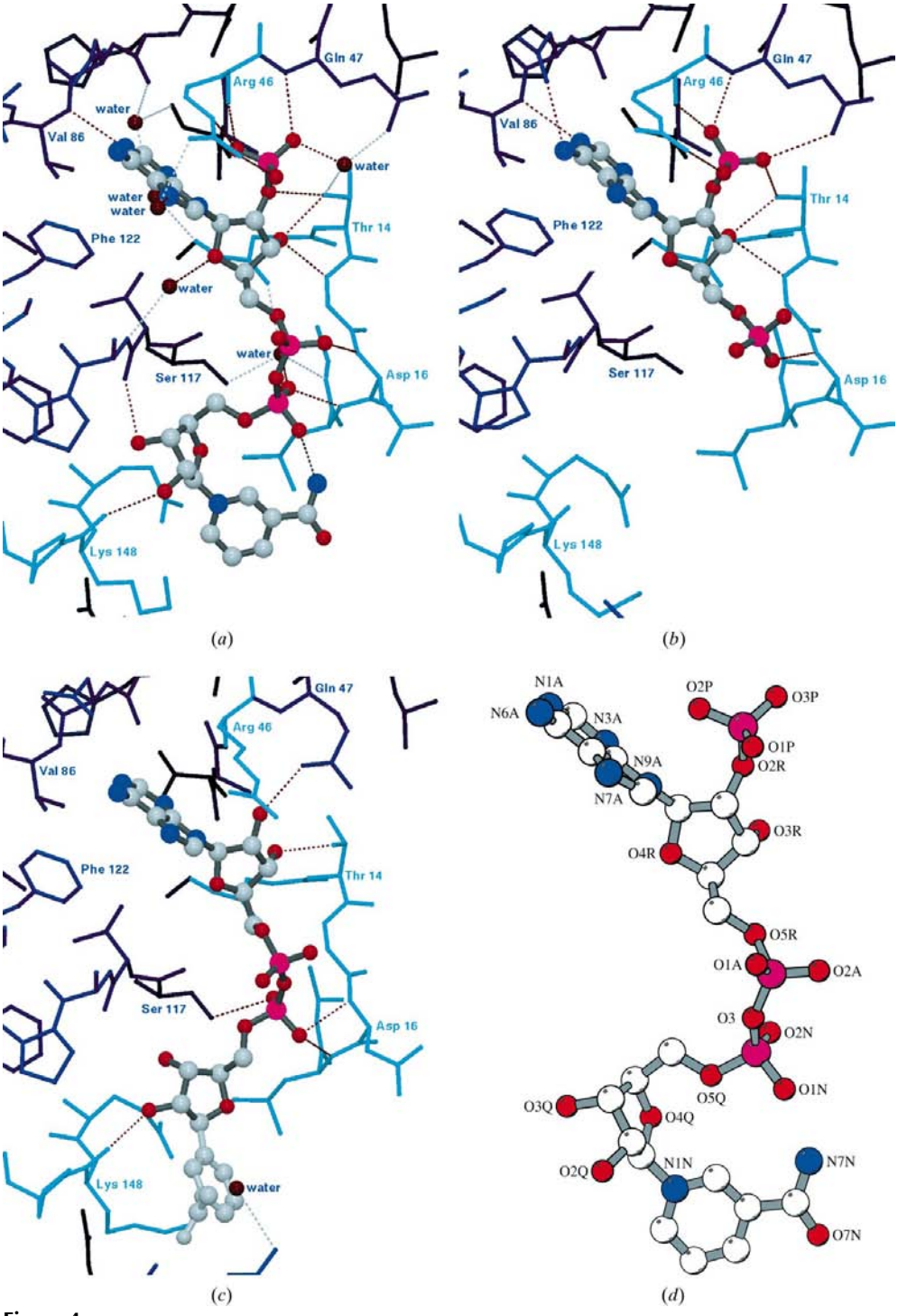

Figure 4
(*a*) Protein–$NADP^+$ contacts, (*b*) protein–NADPH contacts, (*c*) protein–NAD^+ contacts. Coenzymes are shown with C atoms grey, N atoms blue, O atoms red and P atoms purple; waters are red-brown. (Atoms and bonds of the nicotinamide ring of NAD^+ are shown in white to indicate disorder.) Conserved protein residues are cyan; others are dark blue. Possible hydrogen bonds are drawn dotted in red; waters and certain residues discussed are labelled. (*d*) Atom-labelling convention for coenzyme.

Table 4
Mean main-chain differences (Å) between structures with $\beta + \alpha$ domains optimally superposed.

		NAD	*C*2-empty	NADPH–G6P	Subunit AP	Subunit BP
NADP	Overall, scalar	0.52	0.65	0.68	0.66	0.84
	$\beta + \alpha$ domain, scalar	0.30	0.35	0.39	0.26	0.25
	Small domain, scalar	0.89	1.18	1.18	1.34	1.87 (1.90)
	Small domain, vector†	0.39	0.85	0.90	1.11	1.01 (1.41)
NAD	Overall, scalar		0.44	0.47	0.53	0.70
	$\beta + \alpha$ domain, scalar		0.30	0.33	0.27	0.35
	Small domain, scalar		0.67	0.70	0.98	1.32 (1.28)
	Small domain, vector		0.57	0.59	0.79	0.78 (1.02)
*C*2-empty	Overall, scalar			0.20	0.40	0.59
	$\beta + \alpha$ domain, scalar			0.18	0.28	0.37
	Small domain, scalar			0.25	0.62	0.99 (0.86)
	Small domain, vector			0.11	0.30	0.49 (0.60)
NADPH-G6P	Overall scalar				0.46	0.69
	$\beta + \alpha$ domain, scalar				0.31	0.43
	Small domain, scalar				0.72	1.13 (1.00)
	Small domain, vector				0.21	0.58 (0.69)
Subunit AP	Overall scalar					0.62
	$\beta + \alpha$ domain, scalar					0.31
	Small domain, scalar					1.16 (1.02)
	Small domain, vector					0.69 (0.71)

† 'Scalar difference' indicates the mean value of the difference between equivalent main-chain atoms on the alignment concerned. 'Vector difference' indicates the resultant of the vectors between equivalent main-chain atoms of the two domains being considered. A large ratio of vector to scalar difference implies a concerted movement. The direction of the resultant vector indicates the direction of any concerted movement.

nicotinamide ring optimally for hydride transfer. In both NADP and NAD structures, the nicotinamide ribose makes a hydrogen bond to residue 148 of the conserved 147–149 (EKP) turn. In both structures, residues of this turn appear to restrict access of the nicotinamide ring to the 1-carbon of the substrate.

Several authors have addressed discrimination between $NADP^+$ and NAD^+ using structural comparisons or site-directed mutagenesis. Early discussions include those by Wierenga *et al.* (1985, 1986), Scrutton *et al.* (1990) and Baker *et al.* (1992, 1993). In a study of several well refined structures, Carugo & Argos (1997*a*,*b*) have drawn attention to the much greater differences between bound $NADP^+$ conformations than bound NAD^+ conformations. The binding sites of the different proteins inevitably reflect these differences. Comparison of $NADP^+$ bound to G6PD with a non-redundant subset of the proteins considered above showed its conformation to be closest to a group of pro-*S* NAD^+ enzymes such as glyceraldehyde 3-phosphate dehydrogenase (GAPDH; PDB code 1gd1), which like G6PD have complete Rossmann folds. Among $NADP^+$ enzymes, $NADP^+$ bound to G6PD is different from $NADP^+$ bound to dihydrofolate reductase (PDB code 8dfr) without a full Rossmann fold, but more like $NADP^+$ in 6PGDH (PDB code 1pgn) with a full Rossmann fold. While there are some differences between the conformations of NAD^+ and $NADP^+$ when bound to G6PD, NAD^+ bound to G6PD is again similar to NAD^+ bound to GAPDH.

Nonetheless, it is clear that G6PD has the most common characteristic of $NADP^+$-binding enzymes, namely an arginine which interacts with both the 2′-phosphate and the adenine ring. The correct orientation of this residue is normally required before any binding site for the adenine ring is established. It would appear that the range of other residues around the adenine nucleotide of *L. mesenteroides* G6PD allow a (poor) adenine site to be formed even if the arginine is not ordered. Since the interactions depend on several residues which are not conserved, dual specificity is observed in *L. mesenteroides* G6PD but not in the enzyme from most other species.

4.2.1. Implications for mechanism of *L. mesenteroides* G6PD. Nine subunit types have now been observed crystallographically for *L. mesenteroides* G6PD complexes (Fig. 5). Five have been described in this paper: (i) 'empty-open' with sulfate at the outer anion-binding site, (ii) 'open' with $NADP^+$ bound and a sulfate at the outer anion site, (iii) 'half-open' with NAD^+ bound, (iv) 'closed' with no coenzyme and no anion bound and (v) a 'closed' NADPH–G6P complex. The remainder are (vi) a 'closed' binary G6P complex, (vii) 'half-open' D177N-nad G6PD with minimal NAD^+ bound, (viii) the 'closed' AP subunit with the outer and inner phosphate sites occupied and (ix) the 'further closed' BP subunit with Pro149 *trans* and the inner phosphate site occupied.

$NADP^+$ will not bind to either 'closed' subunit of G6PD-P; each has a phosphate ion bound to His178 $N^{\delta1}$ at the inner phosphate site. In crystal soaking experiments, crystals were seen to crack in the presence of high concentrations of coenzyme. It is not possible to say whether the disruption of crystal contacts is caused by the necessity of opening the hinge angle in subunit *A* or by further conformation changes which might be required for $NADP^+$ to bind to subunit *B*. NADPH will bind to a closed G6PD in the presence of G6P, with the phosphate bound to His178 $N^{\varepsilon2}$, but the nicotinamide nucleotide is disordered in this complex.

We suggest that the 'open' form of *L. mesenteroides* G6PD is the form with the tightest binding of $NADP^+$ in a binary complex. Good interactions with $NADP^+$ are achieved by the rotation of the coenzyme domain sheet allowing the βB–αb turn to attain the conformation for optimal interaction of Arg46 with the 2′-phosphate and the adenine ring. In this form, the adenine and nicotinamide ribose moieties hydrogen bond residues at the C-terminus of β-sheet strands. The nicotinamide ring is not completely ordered and the distance between the hydride receptor (C4N) and the base (His240 $N^{\varepsilon2}$) is too large for direct hydrogen transfer from the substrate. A further change in conformation of the complex is therefore required before the reaction can take place. In the more poorly ordered NADPH in the closed ternary complex, Arg46 is less well oriented; hence, the adenine and 2′-phosphate are less well bound. The slightly different orientation

with respect to the enzyme appears to lead to disorder of the whole nicotinamide nucleotide.

There is fluorescence evidence of a conformation change when G6P binds (Haghighi & Levy, 1982); we suggest this is likely to be the open to closed conformation change and that it can also be driven by inorganic phosphate. Kinetic evidence indicates the $NADP^+$-dependent pathway is ordered, with coenzyme binding first. We, therefore, propose that the conformation change would allow the nicotinamide ring of the already bound $NADP^+$ to assume the position from which the active complex for catalysis can be reached. However, if substrate has already bound, $NADP^+$ may be prevented by its tight binding at the 2′-phosphate from reorienting to bind productively to the closed substrate-bound subunit; the nicotinamide nucleotide might then be disordered as is the reduced nicotinamide nucleotide in the ternary complex. Weaker substrate binding may also allow reorientation of the nicotinamide ring; a random mechanism is observed if lysine residues which bind the G6P phosphate are mutated (Vought *et al.*, 2000).

NAD^+ binding is seen in this paper to be incompatible with the 'open' form of the enzyme; the NAD^+ complex is 'half-open'. We suggest that if NAD^+ approaches the 'open' form, it generates a conformation change, initially to the 'half-open' form; the concomitant movement of the coenzyme sheet allows Gln47 to approach the adenine ribose 2′-hydroxyl and moves away the side chain of Arg46. Only the nicotinamide phosphate and ribose are held tightly in the 'half-open' form. They make slightly different contacts to the enzyme from the comparable moieties of $NADP^+$. The orientation is such that were the nicotinamide ordered, it could approach the 1-hydrogen of bound G6P more closely. We predict that substrate could bind to the NAD^+ complex and the subsequent conformation change, for which there is evidence in solution (Haghighi & Levy, 1982), would close the interdomain hinge and allow NAD^+ to reorient to interact better with the protein. Since NAD^+ binding is compatible with a 'half-open' form of the enzyme, it would be possible to bind it either before or after substrate, as indicated by the kinetic mechanism. The poorer order of the adenine nucleotide of NAD^+ compared with that of $NADP^+$ could make conformation changes for productive binding easier to achieve, whether G6P is bound or not.

Ordering of the nicotinamide ring in the position required for reaction and subsequent hydride transfer may not be achieved in the form of the enzyme with Pro149 *cis*. In this conformation, the conserved 147–149 (EKP) turn restricts access of the nicotinamide ring. For correct positioning of the nicotinamide, *cis–trans* isomerization of this peptide bond is likely to be required. The site-directed mutants P149V and P149G, in which the peptide is constrained to be *trans* throughout the reaction, have low activity (Vought *et al.*, 2000). The productive ternary complex is thus likely to be associated with the *cis* to *trans* isomerization of Pro149. This change and the enzyme reaction could be concerted since the main-chain carbonyl of the adjacent residue Lys148 interacts with the nicotinamide ribose and is moved in the *cis–trans* isomerization. Structures of coenzyme and substrate-bound complexes in which Pro149 is *trans* would assist in identifying these further stages.

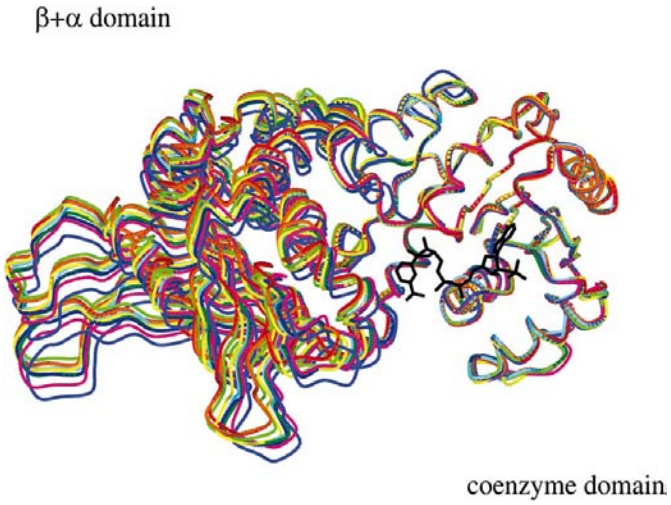

Figure 5
Different *L. mesenteroides* G6PD subunits with the small domains superimposed. Colour code: 'open', NADP orange, $P6_222$-empty red; 'half-open', NAD cream, D177N-nad lime green; 'closed', *C*2-empty dark green, G6P binary blue, NADPH-G6P ternary cyan, subunit AP magenta; 'further closed', subunit BP purple. $NADP^+$ is shown in black.

We are grateful to Professor Louise Johnson for support and facilities in the Laboratory of Molecular Biophysics. We thank the support staff of stations 9.5 and 9.6 at CCLRC Daresbury Laboratory, Warrington, England for facilities and support. CEN was in receipt of a Wellcome Prize Studentship. Part of this work was supported by Grant MCB-9513814 from the National Science Foundation, USA to HRL. MJA is Dorothy Hodgkin–E. P. Abraham Fellow of Somerville College, Oxford and an associate member of the Oxford Centre for Molecular Sciences.

References

Adams, M. J., Basak, A. K., Gover, S., Rowland, P. & Levy, H. R. (1993). *Protein Sci.* **2**, 859–862.
Bacon, D. J. & Anderson, W. F. (1988). *J. Mol. Graph.* **6**, 219–220.
Baker, P. J., Britton, K. L., Rice, D. W., Rob, A. & Stillman, T. J. (1992). *J. Mol. Biol.* **228**, 662–671.
Baker, P. J., Britton, K. L., Rice, D. W., Rob, A. & Stillman, T. J. (1993). *J. Mol. Biol.* **232**, 1012.
Brünger, A. T. (1992*a*). *Nature (London)*, **355**, 472–475.
Brünger, A. T. (1992*b*). *Proceedings of the CCP4 Study Weekend. Molecular Replacement*, edited by E. J. Dodson, S. Gover & W. Wolf, pp. 49–62. Warrington: Daresbury Laboratory.
Brünger, A. T. (1992*c*). *X-PLOR. Version* 3.1. *A System for X-ray Crystallography and NMR.* New Haven, CT, USA/London: Yale University Press.
Camardella, L., Caruso, C., Rutigliano, B., Romano, M., Di Prisco, G. & Descalzi-Cancedda, F. (1988). *Eur. J. Biochem.* **171**, 485–489.
Carugo, O. & Argos, P. (1997*a*). *Proteins*, **28**, 10–28.
Carugo, O. & Argos, P. (1997*b*). *Proteins*, **28**, 29–40.
Collaborative Computational Project, Number 4 (1994). *Acta Cryst.* D**50**, 760–763.
Cosgrove, M. S., Gover, S., Naylor, C. E., Vandeputte-Rutten, L., Adams, M. J. & Levy, H. R. (2000). *Biochemistry*, **39**, 15002–15011.

Cosgrove, M. S., Naylor, C., Paludan, S., Adams, M. J. & Levy, H. R. (1998). *Biochemistry*, **37**, 2759–2767.
De Moss, R. D., Bard, R. C. & Gunsalus, I. C. (1951). *J. Bacteriol.* **62**, 499–511.
Esnouf, R. (1997). *J. Mol. Graph.* **15**, 132–134.
Garman, E. F. & Schneider, T. R. (1997). *J. Appl. Cryst.* **30**, 211–237.
Haghighi, B. & Levy, H. R. (1982). *Biochemistry*, **21**, 6421–6428.
Hurley, J. H., Chen, R. & Dean, A. M. (1996). *Biochemistry*, **35**, 5670–5678.
Jancarik, J. & Kim, S.-H. (1991). *J. Appl. Cryst.* **24**, 409–411.
Jones, T. A. & Kjeldgaard, M. (1997). *Methods Enzymol.* **277**, 173–208.
Kemp, R. G. & Rose, I. A. (1964). *J. Biol. Chem.* **239**, 2998–3006.
Kraulis, P. J. (1991). *J. Appl. Cryst.* **24**, 946–950.
Laskowski, R. A., MacArthur, M. W., Moss, D. S. & Thornton, J. M. (1993). *J. Appl. Cryst.* **26**, 283–291.
Lee, W. T., Flynn, T. G., Lyons, C. & Levy, H. R. (1991). *J. Biol. Chem.* **266**, 13028–13034.
Lee, W. T. & Levy, H. R. (1992). *Protein Sci.* **1**, 329–334.
Levy, H. R. (1979). *Adv. Enzymol. Relat. Areas. Mol. Biol.* **48**, 97–192.
Levy, H. R. (1989). *Biochem. Soc. Trans.* **17**, 313–315.
Levy, H. R., Christoff, M., Ingulli, J. & Ho, E. M. L. (1983). *Arch. Biochem. Biophys.* **222**, 473–488.
Levy, H. R. & Daouk, G. H. (1979). *J. Biol. Chem.* **254**, 4843–4846.
Levy, H. R., Daouk, G., H. & Katopes, M. A. (1979). *Arch. Biochem. Biophys.* **198**, 406–413.
Levy, H. R., Ejchart, A. & Levy, G. C. (1983). *Biochemistry*, **22**, 2792–2796.
Levy, H. R., Vought, V. E., Xiaohong, Y. & Adams, M. J. (1996). *Arch. Biochem. Biophys.* **326**, 145–151.
Merritt, E. A. & Murphy, M. E. P. (1994). *Acta Cryst.* D**50**, 869–873.
Navaza, J. (1994). *Acta Cryst.* A**50**, 157–163.
Otwinowski, Z. & Minor, W. (1997). *Methods Enzymol.* **276**, 307–326.
Read, R. J. (1986). *Acta Cryst.* A**42**, 140–149.
Rosemeyer, M. A. (1987). *Cell Biochem. Funct.* **5**, 79–95.
Rowland, P., Basak, A. K., Gover, S., Levy, H. R. & Adams, M. J. (1994). *Structure*, **2**, 1073–1087.
Scrutton, N. S., Berry, A. & Perham, R. N. (1990). *Nature (London)*, **343**, 38–43.
Tickle, I. J. (1992). *Proceedings of the CCP4 Study Weekend. Molecular Replacement*, edited by E. J. Dodson, S. Gover & W. Wolf, pp. 20–32. Warrington: Daresbury Laboratory.
Vought, V., Ciccone, T., Davino, M. H., Fairbairn, L., Lin, Y., Cosgrove, M. S., Adams, M. J. & Levy, H. R. (2000). *Biochemistry*, **39**, 15012–15021.
Wierenga, R. K., De Maeyer, M. C. H. & Hol, W. G. J. (1985). *Biochemistry*, **24**, 1346–1357.
Wierenga, R. K., Terpstra, P. & Hol, W. G. J. (1986). *J. Mol. Biol.* **187**, 101–107.